Synergistic Integration of Processes Aimed at the Reduction in CO_2 Emissions: Use of Oxyfuel Combustion Ash for the Production of Blended Cements

A. Telesca[*1], M. Marroccoli[1], N. Ibris[1], C. Lupiáñez[2], L. I. Díez[2], L. M. Romeo[2] and F. Montagnaro[3]

[1]*School of Engineering, Università degli Studi della Basilicata, Viale dell'Ateneo Lucano 10, 85100 Potenza, Italy.*

[2]*CIRCE-Universidad de Zaragoza, C/Mariano Esquillor 15, 50018 Zaragoza, Spain.*

[3]*Department of Chemical Sciences, Università degli Studi di Napoli Federico II, Complesso Universitario di Monte Sant'Angelo, 80126 Napoli, Italy.*

Graphical abstract

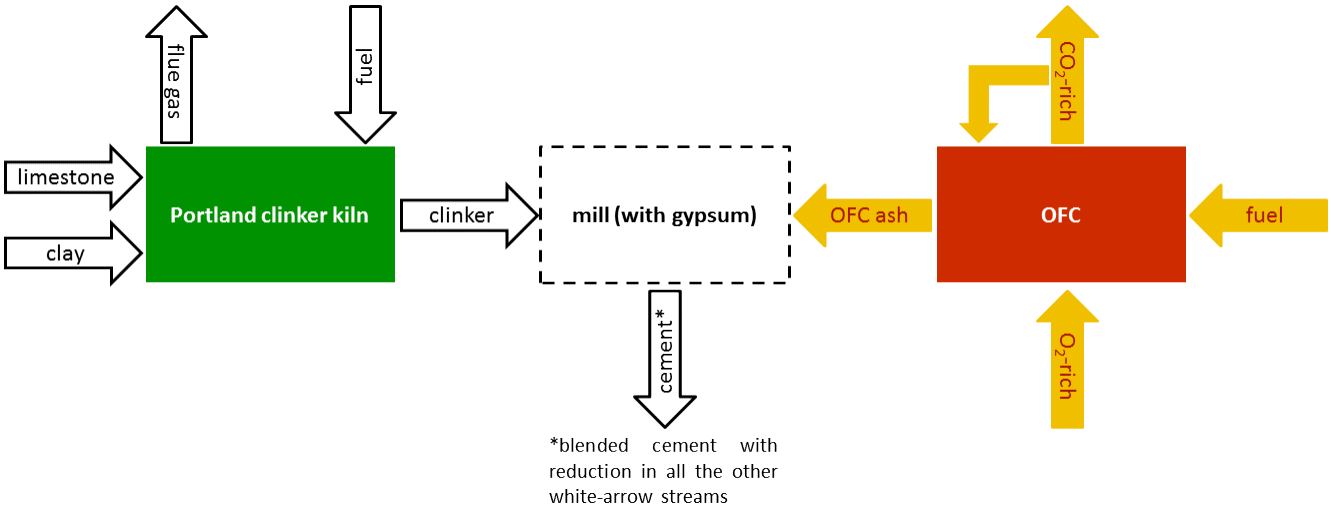

* Corresponding author. T: +39 0971 205225. E-mail: antonio.telesca@unibas.it.

Abstract

In this paper, it is investigated the possibility of reusing ashes issued by an oxyfuel combustion process carried out in a 95 kW_{th} pilot-scale fluidized bed reactor, aimed at mitigating CO_2 emission, in terms of a source of material as substitutes for natural pozzolan in the production of low-CO_2 blended cements. To this end, the oxyfuel plant was operated under controlled conditions by feeding as fuel blends of coal (anthracite or lignite) and biomass (corn stover). Characterization of fly and bottom ashes produced in the plant revealed that the latter showed properties able to make them considerable for the proposed application, to obtain blended cements by mixing them with Portland clinker and natural gypsum. Purposely-conceived blended cements were subjected to pozzolanicity tests, and to hydration for curing times ranging from 2 to 28 d and curing temperatures from 20 to 40°C. X-ray fluorescence and diffraction, differential thermal–thermogravimetric and scanning electron microscopy analyses were employed as characterization techniques. With reference to a standard blended cement, and with particular eye on the blended cement made from bottom ashes obtained when lignite was burnt together with the biomass, a strong similarity in the hydration behavior was observed. It was demonstrated the ability of the silico-aluminous fraction of the oxyfuel bottom ash to react with calcium hydroxide produced by Portland clinker hydration, to yield in particular the desired calcium silicate hydrates among the hydration products. This, as reported in the Graphical Abstract, gives an example for synergistically coupling two different processes both aimed at CO_2 reduction, to convey in a scheme for which savings in the consumption of natural materials/fuels and in the flue gas/ash environmental impact can be achieved as well.

INTRODUCTION

A. Oxyfuel combustion as a mean to reduce CO_2 emissions in the atmosphere

The economic growth during the industrial age has brought exceptional wealth to the humankind, but it has also come at a cost, mainly associated with the current global warming (GW; list of abbreviations reported at the end of the manuscript),[1] representing the main environmental and economic menace in our time.[2] The increase in the average temperature of the Earth's atmosphere as well as its oceans, the melting of permanent snow and polar ice caps, the rise of the mean sea level and the increase of the oceans' acidity together with the occurrence of more violent atmospheric phenomena in recent times represent unequivocal signs of GW;[3,4] this phenomenon is caused by the emissions of greenhouse gases (GHGs) which are mainly released by the burning of fossil fuels, land clearing, agriculture-related and other human activities. The phenomenon of the "climate migrants" from Countries where GW is making the life conditions more and more difficult (namely, considering migration triggered by reasons other than, e.g., political instability) adds to the human and economical cost associated with GW.[5]

Among GHGs, carbon dioxide is the most important and abundant gas giving the largest contribution to GW (65%).[6] Since the beginning of the industrial revolution (around year 1760), the mean concentration of CO_2 in the Earth's atmosphere has increased tremendously, growing from around 280 ppm (the same value as the one estimated around the year 1000 through recent analyses on Antarctic glaciers) to 404.83 ppm (March 2016).[7] In particular, in the decade 2001-2011 the annual average increase in CO_2 emissions was about equal to ca. 4% per year; this value decreased to about 1% per year in the following two years and to about only 0.5% in 2014 when the global CO_2 emissions accounted for 35.7 Gt. At the same time, the world's economy grew by 3%, showing a partial decoupling between the growth in global CO_2 emissions and that in the economy.[8] Almost 61% of CO_2 emission is caused by industrial activities (electricity, heat

generation and other industries).[9] Therefore, searching for promising approaches to mitigate CO_2 emissions represents the priority of studies aimed at mitigating the threat of climate change.

Among the currently developing technologies having the potential to almost completely eliminate CO_2 emissions from power plants and other industries (including cement factories), 'carbon capture and storage [sequestration]' (CCS) processes are of particular relevance.[10–13] CCS indicates a group of technologies developed to obtain CO_2-rich flue gases ready to be stored by injection into geological strata with specific features. Among the different CCS processes, such as e.g. chemical absorption, chemical and calcium looping, oxyfuel combustion (OFC) is of great interest due to its conceptual simplicity.[14] In OFC, a blend of nearly pure oxygen and part of exhaust gas, as O_2 diluent for safety reasons, is used for combustion, thus lowering both nitrogen and NO_x contents in the exhaust gas.[15–17] In absence of the most relevant diluent for CO_2 (namely N_2) and after further treatments, it is possible to obtain streams >90% CO_2-rich .

B. Low-CO_2 blended cements

Cement production is one of the most raw materials- as well as energy-intensive manufacturing processes and represents one of the major industrial sectors giving rise to CO_2 emission. In fact, the contribution to the global anthropogenic CO_2 emission is estimated as high as 7% (namely, about 26% of the industrial CO_2 emission), deriving from a global cement production equal to about 4.3 Gt in 2014.[18,19] Portland cement is the most widely used binder all over the world and is obtained by intergrinding Portland cement clinker (PCC) with a few percent of calcium sulfates (mostly gypsum). PCC is produced by heating and making it to react, in a rotary kiln at about 1450°C, a mixture commonly composed by limestone (about 75%) and clay. For each kg of PCC produced, about 0.87 kg of CO_2 are released;[20] this comes from both limestone thermal decomposition (about 50% of the total CO_2 emission) and fuel combustion

(mainly fossil and pet coke).[21] Therefore, the main challenge of the cement industry is focused on the CO_2 emission reduction to 1.55 Gt per year (about –45% of the current value) by 2050.[20] To this end, since the beginning of the third millennium, both cement producers and scientific community suggested several approaches,[22–25] as: a) the use of non-traditional fuels; b) a higher utilization of low-CO_2 Portland cements; c) the development of alternative low-CO_2 binders obtained from non-Portland clinkers and d) the application of the CCS technology to cement factories.

In particular, low-CO_2 Portland cements, namely hydraulic binders whose production process is associated with a reduced CO_2 generation, can be obtained following two main different approaches:[26,27] 1) the use of a non-carbonated CaO source instead of limestone as a constituent of the Portland clinker-generating raw mix;[28–32] 2) the increased production of blended cements, obtained by mixing Portland clinker with significant amounts of supplementary cementitious materials based on silica and alumina (e.g. natural pozzolans, coal fly-ashes, blast-furnace slags), to alleviate the environmental impact related to the clinker production.[33–37] While the approach 1) has been also dealt with by this research group in the recent past (see e.g. refs.[30,31,38]), the approach 2) is investigated in the present work.

C. Rationale and aim of this work

As a matter of fact, the possibility of reusing ashes issued by an OFC process, aimed at mitigating CO_2 emission, as a source of material in the production of low-CO_2 cements appears surely new in the literature scenario and worthy of investigation, since it is an example for synergistically coupling two different processes both aimed at GHG reduction, to convey in a scheme for which savings in the consumption of natural materials/fuels and in the flue gas/ash environmental impact can be achieved as well (see Graphical Abstract). Accordingly, in this

paper residues generated during an OFC process, carried out in a pilot-scale fluidized bed (FB) reactor, were tested as substitutes for natural pozzolan in blended cements. OFC residues were mixed with an industrial Portland clinker and natural gypsum to evaluate their hydraulic behavior. Another mix, based on natural pozzolan, Portland clinker and natural gypsum was investigated as a reference term. Fratini pozzolanicity tests, together with differential thermal–thermogravimetric (DT–TG), X-ray diffraction (XRD) and scanning electron microscopy (SEM) analyses, were employed to explore the hydration behavior of OFC ashes-based blended cements.

EXPERIMENTAL

Materials and oxyfuel pilot plant

The industrial PCC, natural gypsum (NG) and pozzolan (NP) used in this investigation were supplied by a local cement factory. OFC residues were generated in a 95 kW_{th} oxyfuel FB pilot plant installed at CIRCE, Spain. Figure 1 reports the layout of the experimental plant, which consists of a bubbling FB reactor (2.5 m high with an inner diameter of 21 cm) equipped with two different apparatuses for the removal of fly ash. The FB combustor, cooled by means of a water jacket placed at the bottom of the reactor and four uniformly distributed water-cooled probes, was initially charged with a bed inventory of 5 kg silica sand and fluidized at 0.8 m s^{-1} with a 70% CO_2–30% O_2 flue gas heated (to simulate CO_2 recycle). During the tests, mean bed temperature was 850°C. The fuel and inert bed material feeding system is composed by two hoppers both discharged by two endless screw feeders whose velocity can be independently modified to regulate the desired thermal input. One more endless screw allows to finally inject the fuel into the reactor. A corn stover biomass (B) was mixed with anthracite (A) or lignite (L) in a 20:80 B:A or B:L energy ratio. The measured lower heating value, expressed as kJ kg^{-1}, was

15438, 21620 and 14434 for B, A and L, respectively. Table 1 reports the proximate and ultimate analyses for the employed fuels. As expected, the biomass was characterized by larger volatiles and smaller fixed carbon, ash and sulphur contents with respect to the two fossil fuels. Moreover, a local limestone sorbent (S) was injected into the reactor to capture SO_2 generated during combustion through in situ desulfurization (Ca(in the sorbent):S(in the fuel) inlet molar ratio=2.5). Baffle chamber (BC) and cyclone (CY) apparatuses are employed for fly ash removal. The retained fly ashes are collected in two different deposits and extracted after each experiment. Bottom ashes (BA) are purged from the lower part of the combustor. Full details on the plant can be retrieved elsewhere.[39,40] During each combustion test, three different residues were generated: B/A_BC, B/A_CY and B/A_BA (baffle chamber fly ash, cyclone fly ash and bottom ash, respectively) were residues generated during the combustion of the mixture composed by B and A; B/L_BC, B/L_CY and B/L_BA were those respectively obtained when B and L fuels were burnt (Figure 2). The chemical composition of NG, NP and OFC residues is indicated in Table 2 together with the loss on ignition (l.o.i.) values measured at both 550 and 950°C. Data in Table 2 were obtained through X-ray fluorescence (XRF) analysis. As it will be discussed in the results section, only the 2 bottom ashes showed a chemical composition suitable for further investigation in the proposed application.

Mixtures formulation, pozzolanicity and hydration tests

B/A_BA and B/L_BA were mixed with Portland clinker and natural gypsum, to obtain the related blended cements (termed C_B/A_BA and C_B/L_BA, respectively) whose pozzolanicity and hydration behavior was analyzed. Taking also into account the ashes chemical composition, C_B/A_BA and C_B/L_BA were respectively composed by 61% and 55% Portland clinker, 34% and 40% bottom ashes and 5% NG. Another mix, based on 55% Portland clinker,

40% NP and 5% NG (termed C_R), was employed as a reference Portland blended cement, being this composition the one commonly employed in the industrial practice. To obtain the three blended cements, the three mixes were ground in a laboratory mill to a Blaine fineness equal to 380 $m^2 kg^{-1}$.

The three blended cements were submitted to pozzolanicity tests to evaluate the suitability of the pozzolanic addition to be used in mixture with Portland clinker and natural gypsum. The pozzolanicity is assessed by comparing the concentration of Ca ion expressed as CaO present in the aqueous solution (in contact with the hydrated cement for 8 d at 40°C) with the concentration of Ca ion capable of saturating a solution of the same alkalinity. The blended pozzolanic cement is considered to satisfy the test if the concentration of Ca ion in solution is lower than the saturation concentration. Twenty grams of each cement were added to 100 mL of water and, at the end of the accelerated curing, OH^- and Ca^{++} concentrations were measured according to EN 196-5 standard.[41]

Thereafter, the cements were submitted to hydration tests in order to assess the oxyfuel residues reactivity, namely their ability to react with $Ca(OH)_2$ (produced during the Portland clinker hydration) for generating calcium silicate hydrates and calcium aluminate hydrate which are the typical ordinary Portland cement hydration products. Hydration of the cement pastes (water/cement mass ratio equal to 0.5) was carried out in a thermostatic bath, for curing times ranging from 2 to 28 d at 20 and 40°C. At the end of each aging period, the specimens were (i) pulverized, (ii) treated with acetone (to stop hydration) and diethyl ether (to remove water), (iii) stored in a desiccator over silica gel–soda lime (to ensure protection against H_2O and CO_2) and (iv) submitted to DT–TG and XRD analyses.

Characterization techniques

XRF analysis, used for determining the chemical composition of the investigated materials (Table 2), was performed by means of an energy dispersive BRUKER Explorer S4 apparatus (Maximum power=1 kW; LiF200, PET, OVO-55, OVO-B as analyzed crystals). XRD analysis, utilized for the determination of the mineralogical composition of natural pozzolan, OFC residues and cements hydration products, was performed with a BRUKER D2 PHASER diffractometer (Cu kα radiation and 0.02°2θ s^{-1} scanning rate). The phases involved in qualitative XRD analysis were the following: analcime [$NaAlSi_2O_6 \cdot H_2O$, AMCSD (American Mineralogist Crystal Structure Database) # 0000654)[42], anhydrite ($CaSO_4$, AMCSD # 0005117)[43], augite [$(Ca,Mg,Fe^{2+},Fe^{3+},Al)_2(Si,Al)_2O_6$, AMCSD # 0002990][44], calcite ($CaCO_3$, AMCSD # 0017869)[45], ettringite ($Ca_6Al_2(SO_4)_3(OH)_{12} \cdot 26H_2O$, AMCSD # 0017886)[46], hematite (Fe_2O_3, AMCSD # 0017731)[47], larnite ($2CaO \cdot SiO_2$, AMCSD # 0012179)[48], maghemite (γ-Fe_2O_3, AMCSD # 0007899)[49], portlandite ($Ca(OH)_2$, AMCSD # 0020244)[50], quartz (SiO_2, AMCSD # 0000789)[51].

Simultaneous DT–TG analysis was carried out in a Netzsch Tasc 414/3 apparatus operating in the temperature range 20–1000°C, with a heating rate of 10°C min^{-1}. TG analysis was also used for the quantitative determination of $Ca(OH)_2$ consumed during the pozzolanic reactions. For SEM observations, a FEI Inspect S instrument was used. Specimens were metallized with gold by means of an EMITECH K 550 apparatus.

RESULTS AND DISCUSSION

Characterization of materials

From the chemical composition data listed in Table 2, it is seen that: i) the six OFC ashes

214 can be considered of class F,[52] inasmuch as their silico-aluminous fraction prevails over the
215 calcic one; ii) for the four fly ashes, the l.o.i. at 950°C is not very different from that at 550°C,
216 indicating that this value is mainly related to unburnt carbon (effect already observed at 550°C
217 and confirmed by parallel DT–TG characterization; the additional l.o.i. observed at 950°C is
218 mostly ascribed to the $CaCO_3$ content, originally derived from the limestone used for in situ SO_2
219 capture). In particular, the four fly ashes (B/A_BC, B/A_CY, B/L_BC and B/L_CY) all show a
220 relevant l.o.i, larger than that allowed by the European Standard for the use of fly ash in blended
221 cements (EN 197-1).[53] On the other hand, the two bottom ashes (B/A_BA and B/L_BA) were
222 low in l.o.i. (3.3% and 5.6%, respectively), and this l.o.i. was only detected at 950°C, accordingly
223 with the bed ashes longer mean residence times (i.e. larger carbon burn-off degrees) into the
224 combustor. In addition, the silico-aluminous fraction was relevant in both cases (ca. 80% and
225 67% for B/A_BA and B/L_BA, respectively). The two bottom ashes were therefore characterized
226 by a composition fulfilling the minimal technical requirements prescribed by EN 197-1.

227 To complete the characterization, OFC residues were also submitted to XRD analysis;
228 for all the samples, the main crystalline phase was quartz, with calcite, anhydrite and
229 hematite often detected. Moreover, maghemite (a different crystalline phase of iron oxide) in
230 the samples B/L_BC and B/L_CY was present, in agreement with their high iron content
231 reported in Table 2. For the sake of the simplicity, in Figure 3 only the spectra related to the
232 2 bottom ashes are reported. Apart from quartz and anhydrite detection, it is seen that
233 portlandite in B/A_BA and calcite in B/L_BA samples were present, respectively: portlandite
234 as hydrated lime species, calcite in accordance with the relatively larger l.o.i. content at
235 950°C for B/L_BA.

236 Figure 3 also reports XRD results for NP. Also considering its chemical composition
237 (Table 2), it is seen that the natural pozzolan used in this work has a marked silico-aluminous

238 nature (augite, quartz and analcime were observed in this respect).

239 Figure 4 illustrates the saturation curve together with the indication of the pozzolanicity
240 test results for C_R, C_B/A_BA and C_B/L_BA cements hydrated for 8 d at 40°C, according to
241 EN 196-5. It indicates that the lignite-derived bottom ash residue showed a reactivity similar to
242 that of natural pozzolan; as a matter of fact, both B/L_BA and natural pozzolan satisfied the
243 pozzolanicity test as indicated by the representative points of the related cements (rhombus and
244 rectangle, respectively), located below the saturation curve (zone "1" in Figure 4). On the
245 contrary, the representative point of C_B/A_BA cement is placed above the saturation curve (star
246 in zone "2"), thus highlighting its worse pozzolanicity, most probably due to the low amorphous
247 SiO_2 and Al_2O_3 contents. An analogous result was obtained by pozzolanicity test carried out on
248 the same sample hydrated for 15 d at 40°C.

249

250 **Hydration of blended cements**

251 C_R, C_B/A_BA and C_B/L_BA cements, cured from 2 to 28 d at 20°C and for 8 and 15
252 d at 40°C, were first submitted to DTA-TG analysis. With DT–TG temperature increasing, five
253 endothermal effects were observed and attributed[54] to the following compounds, in the order:
254 calcium silicate hydrate, ettringite, monosulfate, calcium hydroxide and calcium carbonate
255 through the following dehydration endothermal peaks: 99°±8°C, 134°±5°C, 179°±4°C,
256 479°±7°C, 705°±20°C, respectively. As an example, Figures 5 and 6 respectively show the DT–
257 TG thermograms for C_R, C_B/L_BA cement pastes.

258 It is recalled here that: i) calcium silicate hydrates are the main hydration products of the
259 calcium silicates present in the Portland clinker, a process that gives $Ca(OH)_2$ as by-product.
260 Calcium hydroxide, in turn, can react with silica to give more calcium silicate hydrates; ii)
261 calcium trisulfoaluminate (dotriakonta)hydrate (known as ettringite,

262 $3CaO{\cdot}Al_2O_3{\cdot}3CaSO_4{\cdot}32H_2O$) can be formed through the hydration of calcium hydroxide-
263 alumina-calcium sulfate systems; iii) calcium monosulfoaluminate (dodeka)hydrate (known as
264 monosulfate, $3CaO{\cdot}Al_2O_3{\cdot}CaSO_4{\cdot}12H_2O$) can be regarded as the decomposition product of
265 ettringite, in presence of calcium aluminate hydrates and in lack of sulfates. Calcium silicate
266 hydrates are regarded as the main desired hydration product in the cement hydration process.

267 When compared to the reference cement, the thermograms of all the cement pastes based
268 on OFC ashes showed a strong qualitative similarity thus highlighting the OFC bottom ashes
269 feature of acting as reactive cementitious materials. Among the thermograms, the main
270 difference concerned the presence of monosulfate in C_R and C_B/A_BA (and not in
271 C_B/L_BA) which formed already at early curing ages. The absence of this secondary hydration
272 product when dealing with C_B/L_BA could be ascribed to B/L_BA larger sulfate content (see
273 Table 1): this could make ettringite more stable and then less prone to decompose toward
274 monosulfate. A particular feature of C_B/L_BA was to exhibit two different endothermal peaks
275 related to the decomposition of calcium carbonate.

276 Calcium hydroxide concentration *vs.* curing time (20°C) for the three hydrating systems is
277 reported in Figure 7. According to what previously observed, a low $Ca(OH)_2$ concentration is an
278 index of a good system hydration reactivity toward calcium silicate hydrates. Therefore, when
279 compared with the reactivity of the anthracite-derived ash, that of both natural pozzolan and
280 lignite-derived ash appears more satisfying, as arising from both the lower absolute $Ca(OH)_2$
281 concentration values and the decrease of its concentration as curing time increases. Particularly
282 interesting is the similarity between the behaviour of the reference cement and that of C_B/L_BA
283 cement. These results are in agreement with the pozzolanicity test, and again qualify the lignite-
284 derived OFC ash as an interesting material for cementitious applications.

285 The similarity between the reference cement and those OFC ashes-based was also

confirmed by XRD results on the hydrated systems. As an example, XRD patterns for C_R and C_B/L_BA (different curing times, 20°C) are illustrated in Figure 8. Peaks for ettringite and portlandite as hydration products, and quartz, larnite, calcite and anhydrite as raw cement materials, were observed. In particular, due to the pozzolanic activity of both natural pozzolan and lignite-derived oxyfuel residue, the decrease of the portlandite peak intensity is easily observed with the increase of curing time (see for example peaks around 18°2θ).

In Figure 9, SEM micrographs for hydrated C_R and C_B/L_BA (b) cements are reported at 28 days of curing. In both systems the surface of Portland clinker grains is coated by small particles of its main hydration product (CSH); crystals of ettringite are also detected.

In conclusion, results reported in this paper highlight that OFC residues contain silico-aluminous components able to combine with calcium hydroxide generated during Portland clinker hydration. These by-products are very interesting since their utilization as secondary cementitious materials, in addition to the saving of raw materials, allows a clinker dilution which implies a decreased emission of CO_2 and pollutants as well as an increased energy saving per unit mass of cement. It has been found that, despite the high silica content, biomass–lignite bottom ash satisfied the pozzolanicity test, at odds with what observed for biomass–anthracite bottom ash. Nevertheless, by following the hydration behavior through thermal, chemical and diffractometric analyses as well as SEM observations, similarities were displayed by the two investigated blended cements when compared to the reference cement. Forthcoming activity is therefore going to investigate in more detail the process idea proposed in this paper. In fact, the possibility of integrating these two processes (oxyfuel combustion and production of low-CO_2 cements), very different from each other but both devoted to limit the emission of greenhouse gas, together with the reuse of industrial solid wastes, appears very interesting from both the technical and environmental point of view.

REFERENCES

1. Ming, T.; de_Richter, R. K.; Liu, W.; Caillol, S. Fighting global warming by climate engineering: is the Earth radiation management and the solar radiation management any option for fighting climate change? *Renew. Sust. Energ. Rev.* **2014**, *31*, 792-834.
2. Benhelal, E.; Zahedi, G.; Shamsaei, E.; Bahadori, A. Global strategies and potentials to curb CO_2 emissions in cement industry. *J. Clean. Prod.* **2013**, *51*, 142-161.
3. Zhang, X. F.; Zhang, S. Y.; Hu, Z. Y.; Yu, G.; Pei, C. H.; Sa, R. N. Identification of connection units with high GHG emissions for low-carbon product structure design. *J. Clean. Prod.* **2012**, *27*, 118-125.
4. *Climate change 2014: Synthesis Report*; Intergovernmental Panel on Climate Change (IPCC), 2015.
5. *The Human Cost of Weather Related Disasters 1995-2015;* The United Nations Office for Disaster Risk Reduction & Centre for Research on the Epidemiology of Disasters, 2015, http://www.unisdr.org/2015/docs/climatechange/COP21_WeatherDisastersReport_2015_FINAL.pdf.
6. de_Richter, R. K.; Ming, T.; Caillol, S.; Liu, W. Fighting global warming by GHG removal: destroying CFCs and HCFCs in solar-wind power plant hybrids producing renewable energy with no-intermittency. *Int. J. Greenh. Gas Control* **2016**, in press: DOI 10.1016/j.ijggc.2016.02.027.
7. *Trends in atmospheric carbon dioxide;* Global Monitoring Division. Earth System Research Laboratory, March 2016; http://esrl.noaa.gov/gmd/ccgg/trends/.
8. Olivier, J. G. J; Janssens-Maenhout, G.; Muntean, M.; Peters, J. A. H. W. *Trends in global CO_2 emissions: 2015 Report;* PBL Netherlands Environmental Assessment Agency and European Commission Joint Research Centre-Institute for Environment and Sustainability,

2015; www.edgar.jrc.ec.europa.eu www.jrc.ec.europa.eu.

9. *CO_2 emissions from fuel combustion highlights;* IEA; 2010; www.iea.org/co2highlights.

10. Herzog, H.; Eliasson, B.; Kaarstad, O. Capturing greenhouse gases. *Sci. Am.* **2000**, *282*, 72-79.

11. Herzog, H. J. What future for carbon capture and sequestration? *Environ. Sci. Technol.* **2001**, *35*, 148A-153A.

12. Boot-Handford, M. E.; Abanades, J. C.; Anthony, E. J.; Blunt, M. J.; Brandani, S.; Mac Dowell, N.; Fernández, J. R.; Ferrari, M. C.; Gross, R.; Hallett, J. P.; Haszeldine, R. S.; Heptonstall, P.; Lyngfelt, A.; Makuch, Z.; Mangano, E.; Porter, R. T. J.; Pourkashanian, M.; Rochelle, G. T.; Shah, N.; Yao, J. G.; Fennell, P. S. Carbon capture and storage update. *Energ. Environ. Sci.* **2014**, *7*, 130-189.

13. Leung, D. Y. C.; Caramanna, G.; Maroto-Valer, M. M. An overview of current status of carbon dioxide capture and storage technologies. *Renew. Sust. Energ. Rev.* **2014**, *39*, 426-443.

14. Díez, L. I.; Lupiáñez, C.; Guedea, I.; Bolea, I.; Romeo, L. M. Anthracite oxy-combustion characteristics in a 90 kW_{th} fluidized bed reactor. *Fuel Process. Technol.* **2015**, *139*, 196-203.

15. Lupiáñez, C.; Díez, L. I.; Romeo, L. M. NO emissions from anthracite oxy-firing in a fluidized-bed combustor: effect of the temperature, limestone, and O_2. *Energ. Fuel.* **2013**, *27*, 7619-7627.

16. Lupiáñez, C.; Díez, L. I.; Romeo, L. M. Influence of gas-staging on pollutant emissions from fluidized bed oxy-firing. *Chem. Eng. J.* **2014**, *256*, 380-389.

17. Buhre, B. J. P.; Elliott, L. K.; Sheng, C. D.; Gupta, R. P.; Wall, T. F. Oxy-fuel combustion technology for coal-fired power generation. *Prog. Energ. Combust. Sci.* **2015**, *31*, 283-307.

18. Shen, W.; Cao, L.; Li, Q.; Zhang, W.; Wang, G.; Li, C. Quantifying CO_2 emissions from China's cement industry. *Renew. Sust. Energ. Rev.* **2015**, *50*, 1004-1012.
19. *Activity report 2014.* The European Cement Association, 2015; http://www.cembureau.be/.
20. Barcelo, L.; Kline, J.; Walenta, G.; Gartner, E. Cement and carbon emissions. *Mater. Struct.* **2014**, *47*, 1055-1065.
21. Xu, D.; Cui, Y.; Li, H.; Yang, K.; Xu, W.; Chen, Y. On the future of Chinese cement industry. *Cem. Concr. Res.* **2015**, *78*, 2-13.
22. Juenger, M. C. G.; Winnefeld, F.; Provis, J. L.; Ideker, J. H. Advances in alternative cementitious binders. *Cem. Concr. Res.* **2011**, *41*, 1232-1243.
23. Gartner, E.; Hirao, H. A review of alternative approaches to the reduction of CO_2 emissions associated with the manufacture of the binder phase in concrete. *Cem. Concr. Res.* **2015,** *78*, 126-142.
24. Kurtis, K. E. Innovations in cement-based materials: addressing sustainability in structural and infrastructure applications. *Mater. Res. Soc. Bull.* **2015**, *40*, 1102-1108.
25. Schneider, M. Process technology for efficient and sustainable cement production. *Cem. Concr. Res.* **2015,** *78*, 14-23.
26. Pace, M. L.; Telesca, A.; Marroccoli, M.; Valenti, G. L. Use of industrial byproducts as alumina sources for the synthesis of calcium sulfoaluminate cements. *Environ. Sci. Technol.* **2011**, *45*, 6124-6128.
27. Telesca, A.; Marroccoli, M.; Tomasulo, M.; Valenti, G. L.; Dieter, H.; Montagnaro, F. Low-CO_2 cements from fluidized bed process wastes and other industrial by-products. *Combust. Sci. Technol.* **2016**, *188*, 492-503.
28. Bernardo, G.; Marroccoli, M.; Nobili, M.; Telesca, A.; Valenti, G. L. The use of oil well-derived drilling waste and electric arc furnace slag as alternative raw materials in clinker

382 production. *Resour. Conserv. Recy.* **2007**, *52*, 95-102.
383 29. Marroccoli, M.; Pace, M. L.; Telesca, A.; Valenti, G. L.; Montagnaro, F. Utilization of coal
384 combustion ashes for the synthesis of ordinary and special cements. *Combust. Sci. Technol.*
385 **2010**, *182*, 588-599.
386 30. Telesca, A.; Calabrese, D.; Marroccoli, M.; Tomasulo, M.; Valenti, G. L.; Duelli (Varela),
387 G.; Montagnaro, F. Spent limestone sorbent from calcium looping cycle as a raw material for
388 the cement industry. *Fuel* **2014**, *118*, 202-205.
389 31. Telesca, A.; Marroccoli, M.; Tomasulo, M.; Valenti, G. L.; Dieter, H.; Montagnaro, F.
390 Calcium looping spent sorbent as a limestone replacement in the manufacture of Portland
391 and calcium sulfoaluminate cements. *Environ. Sci. Technol.* **2015**, *49*, 6865-6871.
392 32. Perejón, A.; Romeo, L. M.; Lara, Y.; Lisbona, P.; Martínez, A.; Valverde, J. M. The
393 calcium-looping technology for CO_2 capture: on the important roles of energy integration
394 and sorbent behavior. *Appl. Energ.* **2016**, *162*, 787-807.
395 33. Bilodeau, A.; Malhotra, V. M. High-volume fly ash system: concrete solution for sustainable
396 development. *ACI Mater. J.* **2000**, *97*, 41-48.
397 34. De Weerdt, K.; Ben Haha, M.; Le Saout, G.; Kjellsen, K. O.; Justnes, H.; Lothenbach, B.
398 Hydration mechanisms of ternary Portland cements containing limestone powder and fly
399 ash. *Cem. Concr. Res.* **2011**, *41*, 279-291.
400 35. Duan, P.; Shui, Z.; Chen, W.; Shen, C. Effects of metakaolin, silica fume and slag on pore
401 structure, interfacial transition zone and compressive strength of concrete. *Constr. Build.*
402 *Mater.* **2013**, *44*, 1-6.
403 36. Wang, S. Quantitative kinetics of pozzolanic reactions in coal/cofired biomass fly ashes and
404 calcium hydroxide (CH) mortars. *Constr. Build. Mater.* **2014**, *51*, 364-371.
405 37. Juenger, M. C. G.; Siddique, R. Recent advances in understanding the role of supplementary

406 cementitious materials in concrete. *Cem. Concr. Res.* **2015**, *78*, 71-80.
407 38. Romeo, L. M.; Catalina, D.; Lisbona, P.; Lara, Y.; Martínez, A. Reduction of greenhouse gas
408 emissions by integration of cement plants, power plants, and CO_2 capture systems. *Greenh.*
409 *Gases Sci. Technol.* **2011**, *1*, 72-82.
410 39. Romeo, L. M.; Díez, L. I.; Guedea, I.; Bolea, I.; Lupiáñez, C.; González, A.; Pallarés, J.;
411 Teruel, E. Design and operation assessment of an oxyfuel fluidized bed combustor. *Exp.*
412 *Therm. Fluid Sci.* **2011**, *35*, 477-484.
413 40. Lupiáñez, C.; Guedea, I.; Bolea, I.; Díez, L. I.; Romeo, L. M. Experimental study of SO_2 and
414 NO_X emissions in fluidized bed oxy-fuel combustion. *Fuel Process. Technol.* **2013**, *106*,
415 587-594.
416 41. EN 196-5, Methods of testing cement. Pozzolanicity test for pozzolanic cements.
417 42. Gatta, G. D.; Nestola, F.; Boffa Ballaran, T. Elastic behavior, phase transition, and pressure
418 induced structural evolution of analcime. *Am. Mineral.* **2006**, *91*, 568-578.
419 43. Hawthorne, F. C.; Ferguson, R. B. Anhydrous sulphates. II. Refinement of the crystal
420 structure of anhydrite. *Can. Mineral.* **1975**, *13*, 289-292.
421 44. Bindi, L.; Safonov, O. G.; Yapaskurt, V. O.; Perchuk, L. L.; Menchetti, S. Ultrapotassic
422 clinopyroxene from the Kumdy-Kol microdiamond mine, Kokchetav Complex, Kazakhstan:
423 occurrence, composition and crystal-chemical characterization. *Am. Mineral.* **2003**, *88*, 464-
424 468.
425 45. Antao, S. M.; Hassan, I. Temperature dependence of the structural parameters in the
426 transformation of aragonite to calcite, as determined from in situ synchrotron powder X-ray-
427 diffraction data. *Can. Mineral.* **2010**, *48*, 1225-1236.
428 46. Goetz-Neunhoeffer, F.; Neubauer, J. Refined ettringite ($Ca_6Al_2(SO_4)_3(OH)_{12}\cdot 26H_2O$)
429 structure for quantitative X-ray diffraction analysis. *Powder Diffr*. **2006**, *21*, 4-11.

47. Finger, L. W.; Hazen, R. M. Crystal structure and isothermal compression of Fe_2O_3, Cr_2O_3, and V_2O_3 to 50 kbars. *J. Appl. Phys.* **1980**, *51*, 5362-5367.
48. Tsurumi, T.; Hiramo, Y.; Kato, H.; Kamiya, T.; Daimon, M. Crystal structure and hydration of belite. *Ceram. Trans.* **1994**, *40*, 19-25.
49. Pecharromán, C.; González-Carreño, T.; Iglesias, J. E. The infrared dielectric properties of maghemite, γ-Fe_2O_3, from reflectance measurement on pressed powders. *Phys. Chem. Miner.* **1995**, *22*, 21-29.
50. Iizuka, R.; Yagi, T.; Komatsu, K.; Gotou, H.; Tsuchiya, T.; Kusaba, K.; Kagi, H. Crystal structure of the high-pressure phase of calcium hydroxide, portlandite: in situ powder and single-crystal X-ray diffraction study. *Am. Mineral.* **2013**, *98*, 1421-1428.
51. Levien, L; Prewitt, C. T.; Weidner, D. J. Structure and elastic properties of quartz at pressure. *Am. Mineral.* **1980**, *65*, 920-930.
52. ASTM C618-15, Specification for coal fly ash and raw or calcined natural pozzolan for use in concrete.
53. EN 197-1, Cement - Part 1: composition, specifications and conformity criteria for common cements.
54. Taylor, H. F. W. Cement chemistry; Thomas Telford: London, U. K., 1997.

Table 1. Proximate and ultimate analyses for B, A and L, mass%.

	B-Corn stover biomass	A-Anthracite	L-Lignite
Proximate analysis			
Moisture	6.18	2.42	13.57
Volatiles	70.68	6.71	25.72
Fixed carbon	17.64	59.57	30.41
Ash	5.50	31.30	30.30
Lower heating value, kJ kg^{-1}	15438	21620	14434
Ultimate analysis			
C	43.3	59.27	40.53
H	5.82	2.01	3.18
N	0.57	0.91	0.28
S	0.11	1.58	6.65
Cl	0.35	–	–

Table 2. Chemical composition of NG, NP and six OFC residues, mass %.

	NG	NP	B/A_BC	B/A_CY	B/A_BA	B/L_BC	B/L_CY	B/L_BA
CaO	34.08	8.03	8.40	12.20	9.04	9.43	10.82	13.27
SiO_2	0.51	59.06	25.66	26.97	71.36	36.75	26.46	56.75
Al_2O_3	0.71	9.67	8.73	12.82	8.25	13.48	13.76	10.65
Fe_2O_3	0.30	5.22	3.08	5.75	2.16	19.71	20.31	5.51
K_2O	–	1.34	2.57	2.95	2.11	1.31	1.57	1.30
MgO	0.20	1.83	0.88	2.03	0.33	0.94	1.50	0.30
MnO	–	–	0.02	0.03	0.01	0.03	0.04	0.01
Na_2O	–	1.66	0.37	0.77	0.14	0.07	0.10	0.03
P_2O_5	–	–	0.42	0.87	0.04	0.24	0.42	0.06
SO_3	44.37	0.15	1.09	1.85	1.02	3.53	4.15	3.96
TiO_2	–	–	0.47	0.63	0.36	0.47	0.58	0.30
l.o.i.[#]	n.a.	n.a.	41.60	27.90	–	9.80	13.50	–
l.o.i.*	19.02	11.30	47.70	31.20	3.30	11.60	17.50	5.60
Total	99.19	98.26	99.39	98.07	98.12	97.56	97.21	97.74

[#]Loss on ignition at 550°C; *loss on ignition at 950°C.

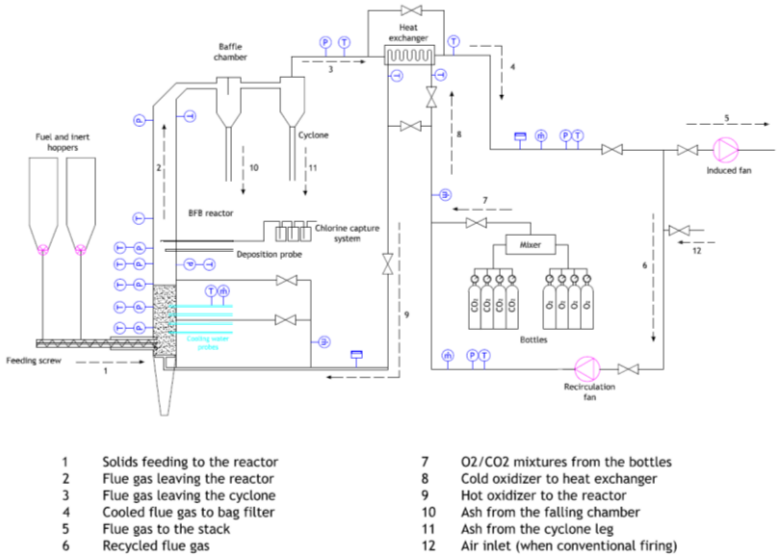

Figure 1. Oxyfuel fluidized bed pilot plant installed at CIRCE, Spain.

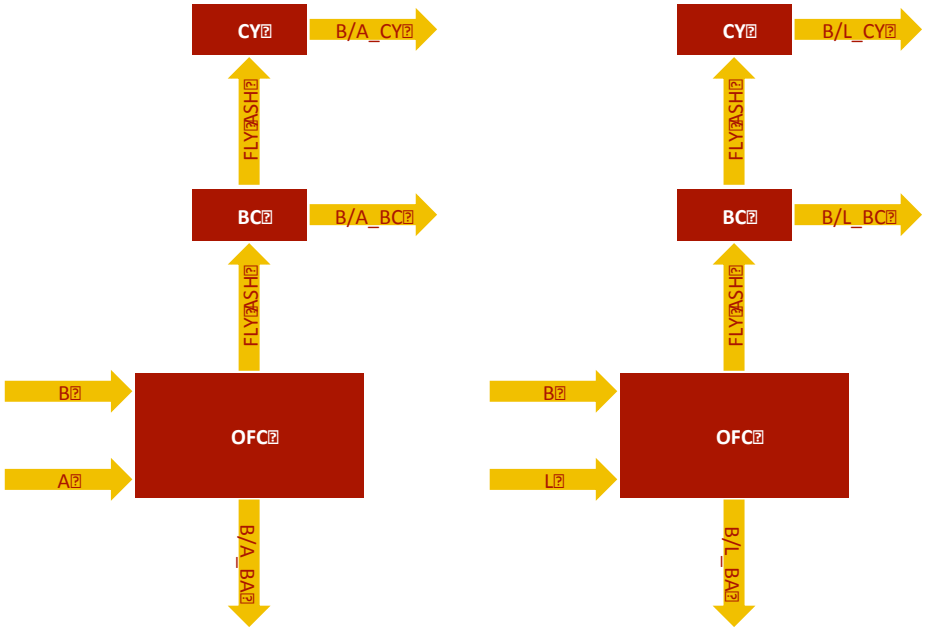

Figure 2. Notation for fly and bottom ashes issuing from the OFC system when biomass is fired with anthracite (left) or lignite (right). List of abbreviations at the end of the manuscript.

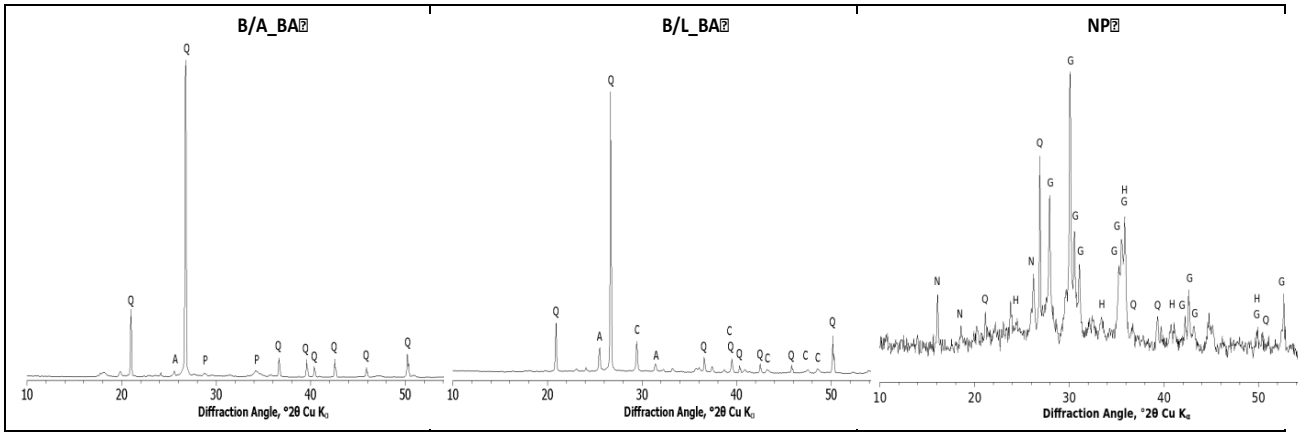

Figure 3. XRD patterns for B/A_BA (top), B/L_BA (middle) and NP (bottom). Legend to symbols: N=analcime; A=anhydrite; G=augite; C=calcite; H=hematite; P=portlandite; Q=quartz.

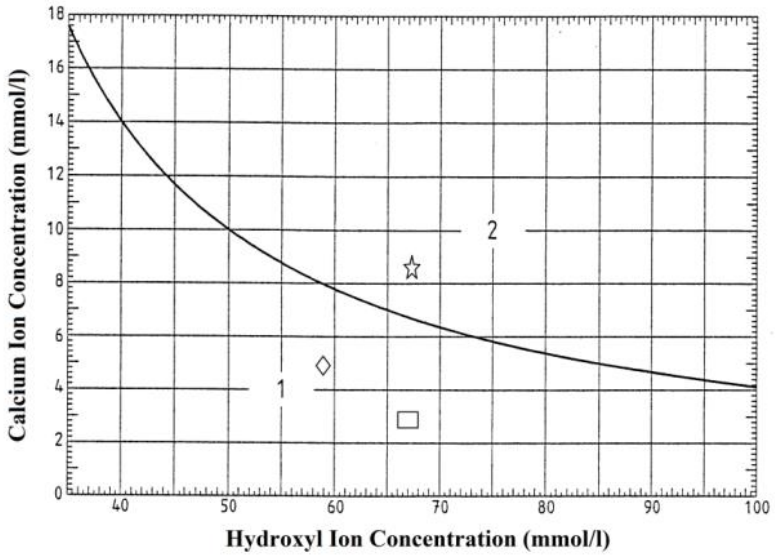

Figure 4. Saturation curve at 40°C together with the indication of the pozzolanicity test results for C_R (rectangle), C_B/A_BA (star) and C_B/L_BA (rhombus) cements. Zone "1" represents the domain in which the test "passes", zone "2" where it "fails".

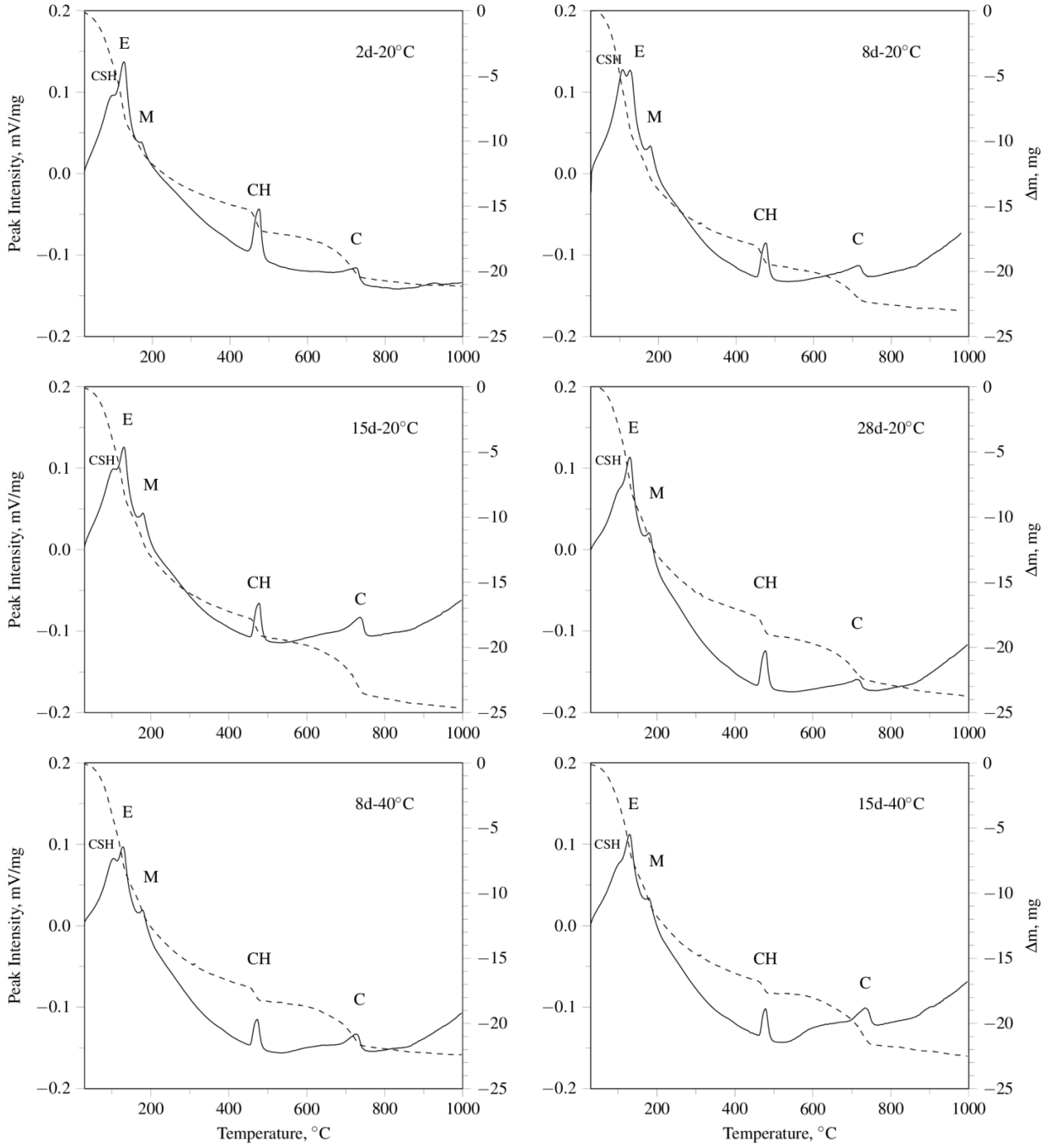

Figure 5. DT–TG thermograms for the reference C_R cement hydrated at 20°C for 2, 8, 15 and 28 d and at 40°C for 8 and 15 d. Legend to symbols: CSH=calcium silicate hydrate; E=ettringite; M=monosulfate; CH=calcium hydroxide; C=calcium carbonate. DT=continuous curve, left-hand y-axis; TG=dashed curve, right-hand y-axis.

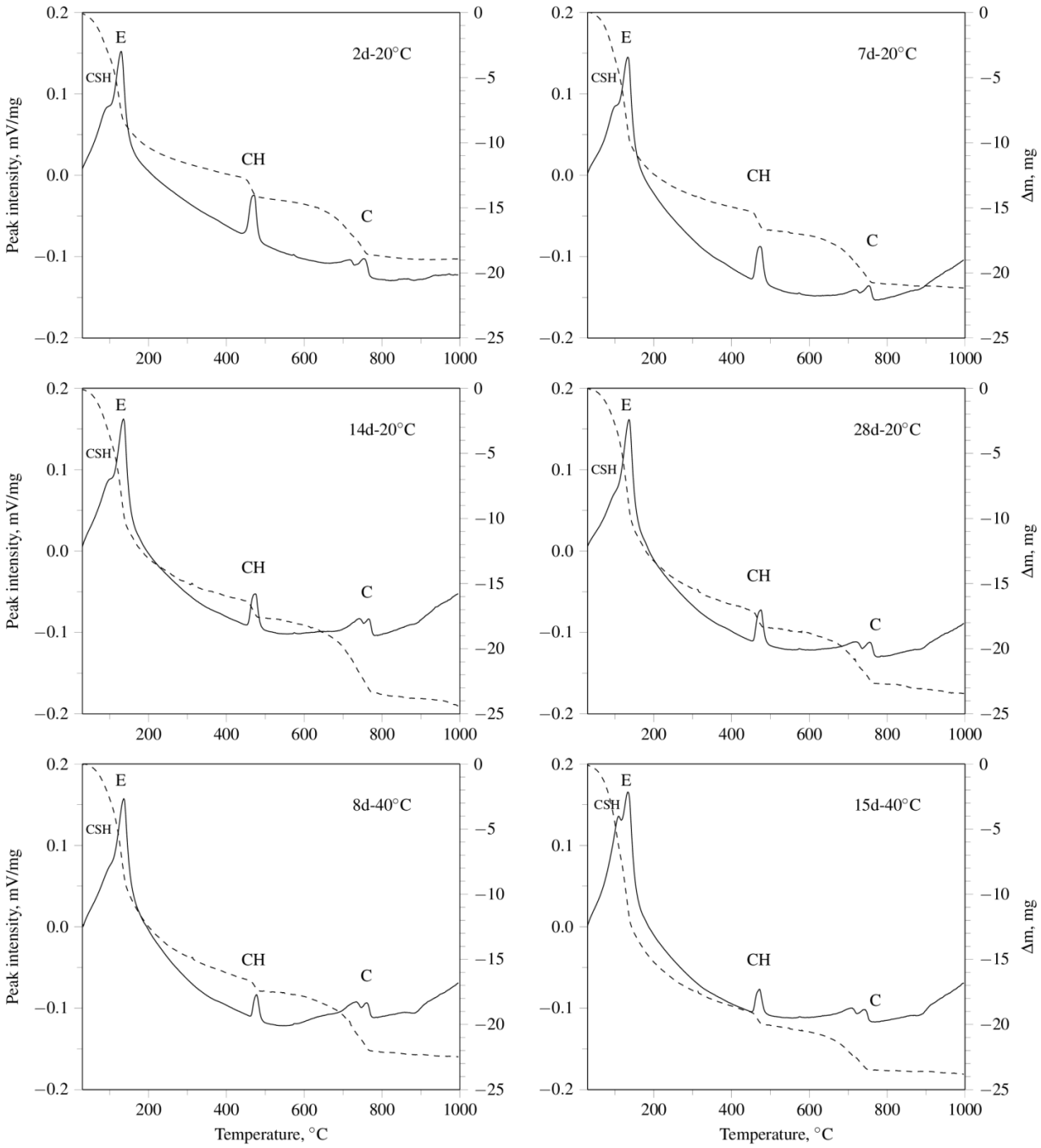

Figure 6. DT–TG thermograms for C_B/L_BA cement hydrated at 20°C for 2, 7, 14 and 28 d and at 40°C for 8 and 15 d. Same legend as in Figure 5.

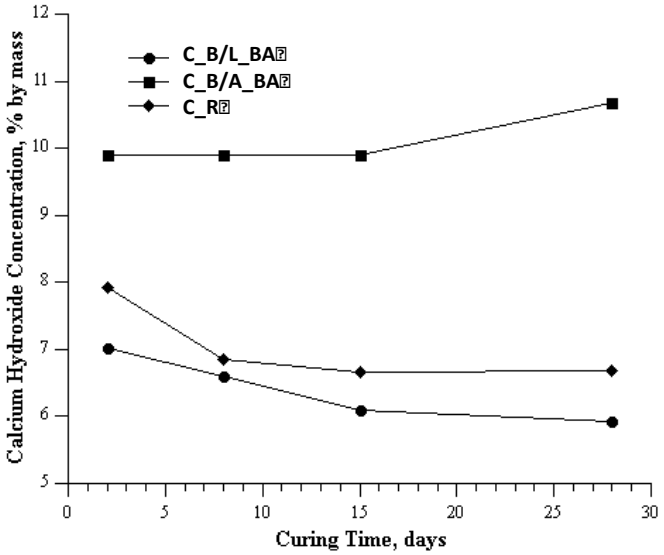

Figure 7. Calcium hydroxide concentration for C_R, C_B/A_BA and C_B/L_BA cements *vs.* curing time at 20°C.

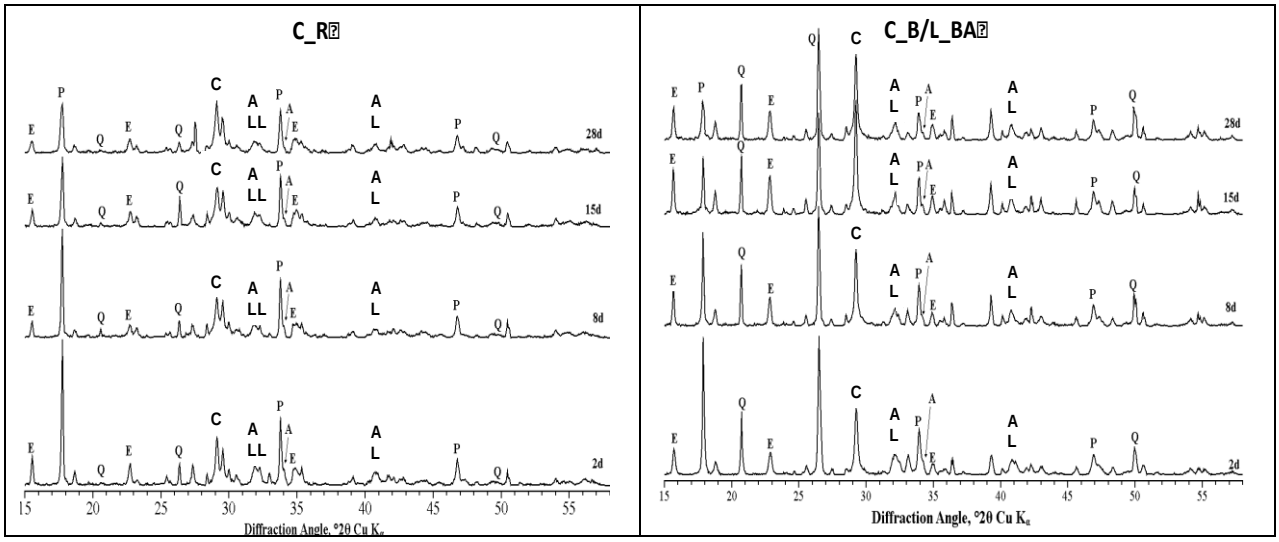

Figure 8. XRD patterns for C_R and C_B/L_BA cements hydrated at 20°C for 2, 8, 15 and 28 d. Legend to symbols: A=anhydrite; C=calcite; E=ettringite; L=larnite; P=portlandite; Q=quartz.

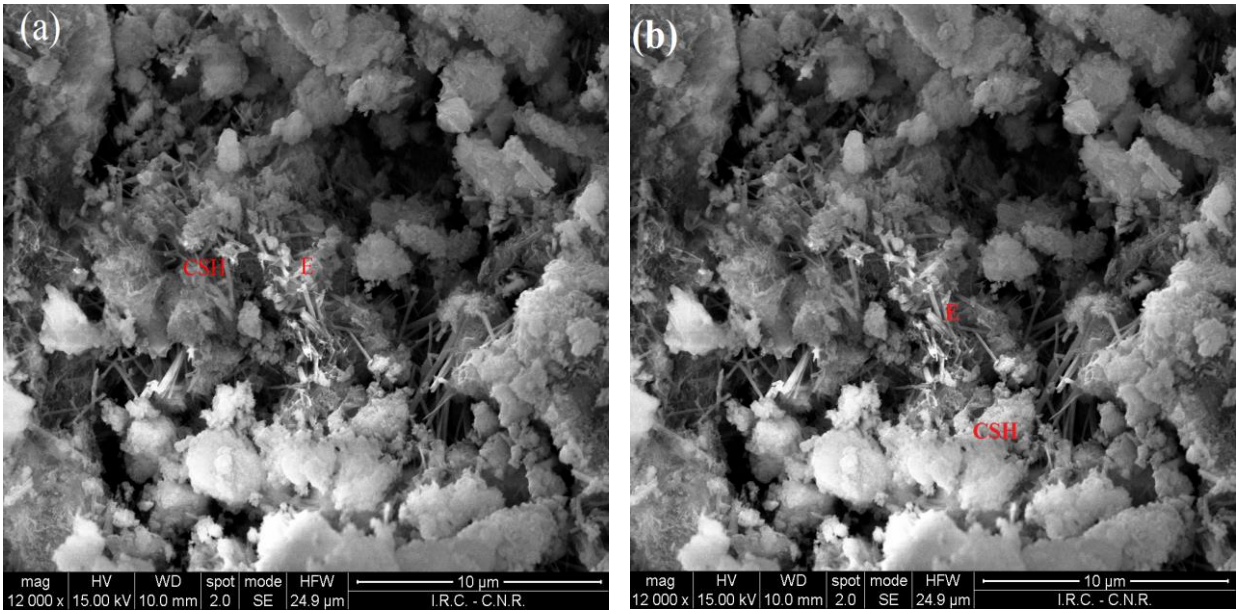

Figure 9. SEM micrographs of C_R (a) and C_B/L_BA (b) cement pastes cured for 28 days at 20°C. E, ettringite; CSH, calcium silicate hydrate.